Published as: *Nat Struct Mol Biol*. 2010 March ; 17(3): 280–288.

Munc13 C_2B-Domain – an Activity-Dependent Ca^{2+}-Regulator of Synaptic Exocytosis

Ok-Ho Shin[1,12,13], **Jun Lu**[2,12,13], **Jeong-Seop Rhee**[6,7,12,13], **Diana R. Tomchick**[2], **Zhiping P. Pang**[1,9], **Sonja Wojcik**[11], **Marcial Camacho-Perez**[7,8], **Nils Brose**[11], **Mischa Machius**[2], **Josep Rizo**[2,3], **Christian Rosenmund**[6,7,8], and **Thomas C. Südhof**[1,4,5,9,10]

[1]Dept. of Neuroscience, UT Southwestern Medical Center, Dallas, TX 75390, USA

[2]Dept. of Biochemistry, UT Southwestern Medical Center, Dallas, TX 75390, USA

[3]Dept. of Pharmacology, UT Southwestern Medical Center, Dallas, TX 75390, USA

[4]Dept. of Molecular Genetics, UT Southwestern Medical Center, Dallas, TX 75390, USA

[5]Howard Hughes Medical Institute, UT Southwestern Medical Center, Dallas, TX 75390, USA

[6]Dept. of Membrane Biophysics, MPI für Biophysikalische Chemie, 37077 Göttingen, Germany

[7]Dept. of Neuroscience, Baylor College of Medicine, Houston TX 77030, USA

[8]Dept. of Molecular & Human Genetics, Baylor College of Medicine, Houston TX 77030, USA

[9]Dept. of Molecular & Cellular Physiology, Stanford University, 1050 Arastradero Rd., CA 94304, USA

[10]Howard Hughes Medical Institute, Stanford University, 1050 Arastradero Rd., CA 94304, USA

[11]Dept. of Molecular Neurobiology, MPI für Experimentelle Medizin, 37075 Göttingen, Germany

Abstract

Munc13 is a multidomain protein of presynaptic active zones that mediates the priming and plasticity of synaptic vesicle exocytosis, but the mechanisms involved remain unclear. Here, we use biophysical, biochemical, and electrophysiological approaches to demonstrate that the central C_2B-domain of Munc13 functions as a Ca^{2+}-regulator of short-term synaptic plasticity. The crystal structure of the C_2B-domain revealed an unusual Ca^{2+}-binding site with an amphipathic α-helix. This configuration confers onto the C_2B-domain unique Ca^{2+}-dependent phospholipid-binding properties favoring phosphatidylinositolphosphates. A mutation that inactivated Ca^{2+}-

Co-corresponding authors (jose@arnie.swmed.edu; rosenmun@bcm.tmc.edu; and tcs1@stanford.edu).
[12]These authors contributed equally
[13]Present addresses: O-H.S., Dept. of Neuroscience & Cell Biology, University of Texas Medical Branch, Galveston, TX 77555-1069; J.L., Jun Lu, Merck & Co. Inc, 126 E. Lincoln Ave., P.O. Box 2000, Rahway, NJ 07065; J-S.R., Dept. of Molecular Neurobiology, MPI für Experimentelle Medizin, 37075 Göttingen, Germany.

AUTHOR CONTRIBUTIONS O.-H. S. performed the protein chemistry and molecular biology experiments, J.L.,D.R.T., and M.M. the structural biology experiments, J.-S.R., and Z.P.P. the electrophysiology experiments, and S.W. and N.B. generated the vectors for expression of mutant Munc13. J.R., C.R., and T.C.S. wrote the paper.

DATA BANK ACCESSION NUMBERS To be added in proofs

dependent phospholipid binding to the C_2B-domain did not alter neurotransmitter release evoked by isolated action potentials, but depressed release evoked by action potential trains. In contrast, a mutation that increased Ca^{2+}-dependent phosphatidylinositolbisphosphate binding to the C_2B-domain enhanced release evoked by isolated action potentials and by action potential trains. Our data suggest that during repeated action potentials, Ca^{2+}- and phosphatidylinositolphosphate-binding to the Munc13 C_2B-domain potentiate synaptic vesicle exocytosis, thereby offsetting synaptic depression induced by vesicle depletion.

INTRODUCTION

Synaptic transmission is initiated when Ca^{2+}-influx during an action potential triggers neurotransmitter release[1]. Synaptic transmission is not a constant point-to-point transfer of information from one neuron to the next, but changes as a function of use, rendering synapses elementary computational units of the brain[2]. Many different types of use-dependent synaptic plasticity have been described, among which presynaptic short-term plasticity stands out because it is universally present at synapses, and can alter synaptic transmission more than 10-fold[3]. Short-term plasticity is of central importance for information processing by the brain; for example, it may underlie working memory formation in cortex[4].

At first approximation, presynaptic short-term plasticity results from two opposing processes[3]. Repeated action potentials deplete the readily-releasable pool (RRP) of synaptic vesicles, thereby inducing synaptic depression. At the same time, Ca^{2+}-influx during repeated action potentials causes accumulation of residual Ca^{2+}, thereby inducing synaptic facilitation. As a consequence, a high release probability usually results in synaptic depression because the RRP becomes depleted, whereas a low release probability usually results in synaptic facilitation because vesicle depletion is delayed but accumulating residual Ca^{2+} increases Ca^{2+}-triggering.

Considerable evidence, however, indicates that presynaptic plasticity is an active, regulated, and synapse-specific process that goes beyond a passive response dictated by the release probability and RRP size. For example, RIM1α and Munc13 are active zone proteins that interact with each other, and form a heterotrimeric complex with the synaptic vesicle protein Rab3[5–9]. Mutations in each of these three proteins induce changes in short-term synaptic plasticity that cannot be accounted for by corresponding alterations in residual Ca^{2+}, release probability, or RRP[8,10–14]. These and other observations indicate that Ca^{2+} not only triggers release, but that during stimulus trains, the residual Ca^{2+} accumulating between action potentials regulates release by independent mechanisms.

At present, the major Ca^{2+}-regulator in short-term synaptic plasticity is thought to be calmodulin[15]. Calmodulin regulates neurotransmitter release by multiple mechanisms, including a direct modulation of Ca^{2+}-channels[16–18], activation of protein kinases[19], regulation of synaptic vesicle priming via the cytoskeleton[20], and binding to Munc13-1 and -2 (13). Moreover, calmodulin acts in presynaptic long-term plasticity by activating adenylate cyclase during mossy-fiber LTP[21,22]. However, the large variety of different types

of presynaptic plasticity with distinct spatio-temporal profiles suggests that calmodulin is unlikely to account for all forms of short-term plasticity.

Munc13s and RIMs are essential for priming synaptic vesicles, and are additionally involved in short- and long-term synaptic plasticity[8,10]. Three Munc13 isoforms (Munc13-1, -2, and -3, of which Munc13-2 is expressed in two principal isoforms called bMunc13-2 and ubMunc13-2) function in synaptic vesicle exocytosis[5,10,23,24]. In addition, two ubiquitously expressed Munc13 isoforms (BAP-3 and Munc13-4 probably act in non-synaptic forms of exocytosis[25–27]. Munc13s have variable N-terminal sequences, but contain similar central and C-terminal domains: a C_2B-domain, a large Munc13-homology region (the MUN domain[14]), and a Ca^{2+}-independent C_2C-domain (Fig. 1A). It seems likely that the canonical Munc13-domains, i.e. their C_2B-, MUN- and C_2C-domains, mediate their shared functions, whereas their variable N-terminal domains modulate these functions. Consistent with this notion, the calmodulin-binding motif and the C_1-domain of Munc13-1 are involved in short-term synaptic plasticity[12,13], whereas its MUN domain mediates its priming function[14,28,29].

The C_2B-domains of all Munc13 isoforms, but not their C_2A- and C_2C-domains, contain the requisite Ca^{2+}-binding residues of C_2-domains[30] (Fig. 1A), suggesting that Munc13's may universally bind Ca^{2+} via their C_2B-domains. However, previous attempts to demonstrate Ca^{2+}-binding to the Munc13 C_2B-domain failed[5]. We now show that the rat Munc13 C_2B-domain binds Ca^{2+}, and contains an unusual α-helix in its top Ca^{2+}-binding loops. The Munc13 C_2B-domain exhibits Ca^{2+}-dependent phospholipid binding with an unexpected PIP- and PIP_2-specificity that differs from that of other C_2-domains, and that mediates the Ca^{2+}-dependent regulation of short-term synaptic plasticity by the Munc13 C_2B-domain. Thus, our data reveal that the Munc13 C_2B-domain functions as a Ca^{2+}-regulator of short-term synaptic plasticity by interfacing with PIP and PIP_2.

RESULTS

The Munc13 C_2B-domain is a Ca^{2+}-binding module

The C_2B-domains of all Munc13 isoforms contain the canonical Ca^{2+}-binding sites of C_2-domains[30] (Fig. 1a), but exhibit only limited sequence homology to other C_2-domains, hindering prediction of domain boundaries. Thus, we first examined the minimum sequence necessary to obtain an autonomously folded Munc13 C_2B-domain, and identified a C_2B-domain fragment that was soluble and monomeric (residues 675–820 in Munc13-1).

To determine whether the C_2B-domain binds Ca^{2+}, we recorded fluorescence spectra of purified C_2B-domains from Munc13-1 and Munc13-2 in the absence or presence of Ca^{2+} or Mg^{2+} (Fig. 1b and Supplementary Fig. 1). For Munc13-2, we also examined a mutant C_2B-domain in which two canonical aspartates (D^{629} and D^{635}) in the presumptive Ca^{2+}-binding sites were replaced by asparagines (referred to as the DN-mutant, Fig. 1a). Application of Ca^{2+} but not Mg^{2+} enhanced the intrinsic fluorescence of the wild-type (WT) C_2B-domains, but had no effect on DN-mutant C_2B-domain, suggesting that the Munc13 C_2B-domains specifically bind Ca^{2+} (Fig. 1b).

We next acquired ^{1}H-^{15}N heteronuclear single quantum correlation (HSQC) spectra of the Munc13-1 C_2B-domain in the absence and presence of Ca^{2+} (Fig. 1c, black and red contours, respectively). Ca^{2+} induced extensive cross-peak changes as expected for a Ca^{2+}-binding module. During Ca^{2+}-titrations, some cross-peaks exhibit progressive Ca^{2+}-induced shifts (e.g. Fig. 1d, upper left corner). Other cross-peaks disappeared during the titration, or shifted to different parts of the spectrum (Figs. 1d and 1e), suggesting that the exchange between Ca^{2+}-free and Ca^{2+}-bound states is slow on the NMR time scale. The curved, progressive Ca^{2+}-induced shifts of some cross-peaks, and the differential shifts between cross-peaks (Figs. 1d and 1e), show that at least two Ca^{2+}-ions bind to the C_2B-domain. At a C_2B-domain concentration of 120 μM, no major cross-peak shifts occurred beyond 250–300 μM Ca^{2+}, demonstrating that Ca^{2+}-binding was saturable. The cross-peak movements can be fitted to a binding model with two Ca^{2+}-binding sites and a K_D of <100 μM.

Crystal structure of Ca^{2+}-free and Ca^{2+}-bound C_2B-domain

To study how Ca^{2+} binds to the Munc13 C_2B-domain, we crystallized the Ca^{2+}-free and Ca^{2+}-bound Munc13-1 C_2B-domain. The Ca^{2+}-free and Ca^{2+}-bound C_2B-domain cystals exhibited distinct space groups ($C222_1$ and $P4_32_12$, respectively). Using diffraction data and the crystal structure of the synaptotagmin-1 C_2A-domain[31] as a search model for molecular replacement, we determined the structure of the Ca^{2+}-free Munc13-1 C_2B-domain to a resolution of 1.90 Å (Table 1). The resulting model was then employed for molecular replacement together with diffraction data to determine the structure of the Ca^{2+}-bound C_2B-domain to a resolution of 1.37 Å (Fig. 2).

The Ca^{2+}-free and Ca^{2+}-bound C_2B-domains contained a typical C_2-domain β-sandwich fold with two four-stranded β-sheets and a type II C_2-domain topology (Figs. 2a and 2b)[32]. Ca^{2+} did not cause major changes in the β-sandwich, as described for synaptotagmin-1 C_2-domains[31],[33],[34], but induced large changes in the top loops. In the Ca^{2+}-free C_2B-domain, substantial parts of loops 1, 3 and 4 exhibited little electron density, indicating that the Ca^{2+}-free loops are disordered (Fig. 2b). In the Ca^{2+}-bound C_2B-domain, however, we observed well-defined electron densities for all four top loops (Figs. 2a and 2b), for two bound Ca^{2+}-ions, and for multiple water molecules (partly illustrated in Fig. 2d). The Ca^{2+}-binding region is likely stabilized by Ca^{2+} binding, similar to the synaptotagmin-1 C_2-domains[33],[34]. In addition, the top loops in the Ca^{2+}-bound C_2B-domain structure were involved in extensive crystal contacts that may have contributed to the stabilization of the top loops.

Structural comparisons using DALI[35] revealed that several structures of other type II C_2-domains in the Protein Data Bank (PDB) exhibited close similarity to the Munc13-1 C_2B-domain, including structures of the C_2-domains from PKCζ, PLC-δ1 and $cPLA_2$ (PDB accession codes 1gmi, 1djx and 1rlw, respectively). However, the lowest rms deviation from the Ca^{2+}-bound Munc13-1 C_2B-domain (1.1 Å for 97 equivalent Cα carbons) was observed for the synaptotagmin-1 C_2A-domain structure (PDB accession codes 1rsy and 1byn), despite the fact that it exhibits a type I topology. Backbone superpositions confirmed the similarity of the synaptotagmin-1 C_2A-domain and the Munc13-1 C_2B-domain (Fig. 2c). Strikingly, the major difference between the Munc13-1 C_2B-domain and all other C_2-

domains is an extended loop 3 of the Munc13 C2B-domain that contains a unique protruding α-helix, and is absent from other C_2-domains (Figs. 2a,f).

Ca^{2+}-binding mode of the Munc13 C_2B-domain

C_2-domains commonly bind two or three Ca^{2+}-ions through five conserved aspartate side chains from loop 1 (aspartates D1 and D2) and loop 3 (aspartates D3–D5)[30,36]. The crystal structure of the Ca^{2+}-bound Munc13-1 C_2B-domain revealed two bound Ca^{2+}-ions (Figs. 2), consistent with the NMR data (Figs. 1d and 1e). The two Ca^{2+}-ions are coordinated by the five canonical aspartate residues, accounting for the block of Ca^{2+}-binding by the DN-mutation (Fig. 1b). In addition, the Ca^{2+}-ions were coordinated by two backbone carbonyl oxygens and two water molecules (Figs. 2d and 2e). Loop 3 of the Munc13-1 C_2B-domain contains additional acidic residues that did not participate in Ca^{2+}-binding but are oriented towards the Ca^{2+}-binding sites, and may increase its Ca^{2+}-affinity (Fig. 2f). Moreover, exposed basic and hydrophobic residues confer an amphipathic character onto the unique α-helix of loop 3 in the Munc13 C_2B-domain. This amphipathic character could be increased by extending the α-helix towards the C-terminus to include R^{769} to R^{772}, and the helical structure may have been partially distorted by crystal contacts (Supplementary Fig. 2). Hence, a longer α-helix spanning residues 762–772 may be formed by loop 3 of the Munc13 C_2B-domain in solution and/or upon binding of the C_2B-domain to phospholipid bilayers (see below).

The Munc13 C_2B-domain is a Ca^{2+}/phospholipid-binding module

We next examined whether Munc13 C_2B-domains bind to phospholipids in a Ca^{2+}-dependent manner. First, we measured fluorescence resonance-energy transfer (FRET) from the Munc13-1 C_2B-domain to dansyl-labeled liposomes containing PIP and PIP_2. Ca^{2+} increased FRET only when both protein and liposomes were present, and this increase was reversed by EGTA (Fig. 3a and Supplementary Fig. 3). FRET may be mediated by the conserved tryptophan residue near loop 3 of the Munc13 C_2B-domain (Fig. 1a), as this residue is in the phospholipid-interacting sequence of C_2-domains.

Next, we employed a centrifugation assay with liposomes containing a synaptic phospholipid composition with 0.5% PIP and 0.1% PIP_2 (ref. 37). Besides the wild-type Munc13-1 and 13-2 C_2B-domains and the DN-mutant Munc13-2 C_2B-domain, we examined an additional Munc13-2 C_2B-domain mutant called the KW-mutant, in which $lysine^{630}$ in loop 1 is exchanged for tryptophan (Fig. 1a). The KW-mutant was designed to render the Munc13 C_2B-domain more similar to the synaptotagmin-1 C_2A-domain. Synaptotagmin-1 contains at this position a hydrophobic methionine (Fig. 1a) that inserts into the phospholipid bilayer in a Ca^{2+}-dependent manner[38], and enhances the Ca^{2+}-dependent phospholipid binding affinity of the synaptotagmin-1 C_2A-domain[39–41]. Tryptophan was used instead of methionine to maximize the membrane penetration of the Munc13 C_2B-domain, as previously shown for the synaptotagmin-1 C_2A-domain[40,41].

The Munc13-1 and 13-2 C_2B-domains bound poorly to synaptic liposomes in the absence of Ca^{2+}, but strongly in the presence of Ca^{2+} (Fig. 3b). Quantitation of Coomassie-blue stained SDS-gels revealed that the Munc13-1 and 13-2 C_2B-domains exhibited similar apparent

Ca^{2+}-affinities (Munc13-1: EC_{50} = 5.5±0.9 μM Ca^{2+} [n=3]; Munc13-2: EC_{50} = 5.3±0.8 μM Ca [n=3]; means ± SEMs) that were indistinguishable from that of the synaptotagmin-1 C_2A/B-domain fragment (EC_{50} = 6.4 ± 0.5 μM Ca^{2+} [n=4; means ± SEMs]; Supplementary Fig. 4). The DN-mutation blocked all Ca^{2+}-dependent phospholipid binding (EC_{50} >1 mM Ca^{2+}), whereas the KW-mutation did not alter the extent or apparent Ca^{2+}-affinity of Ca^{2+}-dependent phospholipid binding under these conditions (EC_{50} = 5.4±0.9 μM Ca^{2+} [n=3; means ± SEM]; Fig. 3b).

Unusual phospholipid specificity of the Munc13 C_2B-domain

We next examined whether decreasing the PIP- and PIP_2-concentrations alters Ca^{2+}-dependent phospholipid binding by wild-type or mutant Munc13 C_2B-domains. An only two-fold decrease of the PIP- and PIP_2-concentrations (to 0.25% PIP and 0.05% PIP_2) abolished Ca^{2+}-dependent liposome binding of the wild-type Munc13 C_2B-domain, but not of the synaptotagmin-1 C_2-domains (Fig. 3c). Strikingly, the KW-mutation converted the Munc13 C_2B-domain into a synaptotagmin-like domain, with full Ca^{2+}-induced binding to the liposomes containing reduced PIP- and PIP_2-concentrations (Munc13-2 KW: EC_{50} = 18.8±2.6 μM Ca^{2+} [n=4]; Syt-1: EC_{50} = 17.2±2.4 μM Ca^{2+} [n=3]; means ± SEMs; Fig. 3c). Thus, the Munc13 C_2B-domain is more sensitive to the PIP- and PIP_2-concentrations than the synaptotagmin-1 C_2-domains, but a single amino-acid substitution renders the lipid-binding properties of the Munc13 C_2B-domain similar to those of synaptotagmin-1.

Assays of Ca^{2+}-dependent binding of wild-type Munc13-2 C_2B-domain to liposomes containing increasing concentrations of PIP or PIP_2 revealed that both phosphatidylinositolphospholipids equally promoted Ca^{2+}-dependent binding (Fig. 4 and Supplementary Fig. 5). This behavior was unexpected because Ca^{2+}-dependent binding of the synaptotagmin-1 C_2-domains to liposomes exhibits a strong preference for PIP_2 due to its higher negative charge[42,43]. Again, the KW-mutant Munc13 C_2B-domain preferentially bound to the PIP_2-containing liposomes, similar to the synaptotagmin-1 C_2-domains (Fig. 4).

In synaptotagmin-1, C_2-domains not only bind to phospholipids, but also to SNARE proteins[43–46]. However, pull-down experiments with solubilized brain proteins uncovered Ca^{2+}-dependent binding of the Munc13 C_2B-domains only to tubulin (which as an abundant protein binds non-specifically to many proteins), but not to SNARE proteins, suggesting that the Munc13 C_2B-domain does not interact with SNARE proteins (Supplementary Fig. 6).

Role of Munc13-2 C_2B-domain in neurotransmitter release

In order to assess the functional importance of Ca^{2+}-binding to the Munc13 C_2B-domain, we analyzed synaptic transmission in autapses formed by hippocampal neurons that were cultured on micro-islands of glia cells. The neurons were isolated from mice that lack Munc13-1 and 13-2, and were rescued by viral expression of the `ubMunc13-2' variant of Munc13-2, used because of its pronounced effects on short-term synaptic plasticity[24,47].

We first analyzed synaptic transmission induced by isolated action potentials. Wild-type, DN-mutant, and KW-mutant Munc13-2 rescued the loss of synaptic transmission induced by deletion of Munc13-1 and 13-2 (Fig. 5a). Rescue with WT and DN-mutant Munc13-2

caused no major change in EPSC amplitudes, whereas rescue with KW-mutant Munc13-2 increased the EPSC amplitudes almost two-fold (Fig. 5b). To test whether this change is due to a difference in the size of the RRP, we measured the RRP by application of hypertonic sucrose[48], but detected no significant change (Fig. 5c). We also determined the vesicular release probability (P_{vr}) for each neuron expressing WT or mutant Munc13-2 by calculating the ratio of integrated EPSC and RRP charges. The DN-mutation did not alter the vesicular release probability, whereas the KW-mutation nearly doubled it (Fig. 5d).

To confirm that the KW- but not the DN-mutation of the C_2B-domain of Munc13 alters the release probability during islated action potentials, we monitored the relative EPSC amplitudes of synapses expressing WT, DN-, or KW-mutant Munc13-2 at low (1 mM) or high (12 mM) extracellular Ca^{2+}-concentrations (Fig. 5e). Consistent with an unchanged basal release probability, WT and DN-mutant Munc13-2 exhibited the same relative Ca^{2+}-dependent changes in ESPC amplitudes. In contrast, KW-mutant Munc13-2 displayed a relative increase in EPSC amplitude at the low ambient Ca^{2+}-concentration, confirming the hypothesis (Fig. 5f).

In increasing release, KW-mutant Munc13-2 could act either as a Ca^{2+}-sensor for triggering release analogous to synaptotagmin, or as an auxiliary Ca^{2+}-regulator of Ca^{2+}-triggering by synaptotagmin. To differentiate between these two possibilities, we tested whether wild-type or KW-mutant Munc13-2 confer Ca^{2+}-triggered neurotransmiter release onto synapses from synaptotagmin-1 KO mice that lack almost all such release[49]. However, neither WT nor KW-mutant Munc13-2 rescued the loss of Ca^{2+}-induced synchronous release in synaptotagmin-deficient synapses, suggesting that Munc13-2 functions as an auxiliary Ca^{2+}-regulator in release (Supplementary Fig. 7).

The Munc13-2 C_2B-domain in short-term plasticity

We next monitored synaptic responses induced by 2.5, 10, and 40 Hz stimulus trains in synapses expressing WT or mutant Munc13-2. Plots of normalized responses revealed that as expected, synapses expressing WT Munc13-2 exhibited strong facilitation at 2.5 Hz stimulation, and less facilitation at 10 Hz stimulation (Figs. 6a–6d; and Supplementary Fig. 8). In contrast, synapses expressing DN- or KW-mutant Munc13-2 both displayed no facilitation, but transient depression during the 2.5 Hz stimulation, and persistent depression during the 10 Hz stimulation (Figs. 6a and 6c).

Strikingly, plots of absolute synaptic responses indicated that the analysis of normalized responses is misleading. Specifically, synapses expressing KW-mutant Munc13-2 started off with a much higher absolute EPSC value than synapses expressing WT Munc13-2, and exhibited continuously larger EPSCs, whereas synapses expressing DN-mutant Munc13-2 stated off with an unchanged EPSC value, but experienced more severe synaptic depression during the stimulus trains (right panels, Figs. 6b and 6d). Thus, in synapses containing KW-mutant Munc13-2, the initially increased release probability leads to a faster depletion of the RRP and apparent depression. In contrast, in synapses expressing DN-mutant Munc13-2, the initial release probability is normal, and depression develops because the accumulating Ca^{2+} that normally augments release by binding to the Munc13 C_2B-domain can no longer bind to the domain.

To confirm these conclusions, we analyzed a second, related form of short-term synaptic plasticity: augmentation of synaptic responses observed after a short high-frequency stimulus train. We measured synaptic responses before and after application of a 5 s, 10 Hz stimulus train and again analyzed normalized and absolute EPSC amplitudes (Figs. 6e and 6f). Plots of normalized responses showed that augmentation was largest in synapses expressing wild-type Munc13-2 (2.3 ± 0.1 fold, n=77), but was impaired in synapses expressing DN- or KW-mutant Munc13-2 (1.3 ± 0.1, n=71, $p<0.001$; 1.5 ± 0.1, n=93, $p<0.001$). Plots of absolute responses, however, showed that DN-mutant expressing synapses exhibited a true loss of augmentation, whereas the apparent loss of augmentation in KW-mutant expressing synapses was not present since the synapses start from an enhanced `plateau' (Fig. 6f). Interestingly, the loss of augmentation in synapses expressing DN-mutant Munc13-2 applied only to the very initial phase; later in the stimulus train, responses recovered, consistent with the notion that multiple Ca^{2+}-regulators mediate augmentation[13,16–20,50].

Our data suggest that the main mechanism by which Ca^{2+}-binding to the Munc13 C_2B-domain mediates synaptic augmentation involves a change in vesicle release probability, as the gain-of-function KW mutant has a two-fold higher initial release probability. To test further whether additional effects on vesicle repriming could explain the phenotype, we measured the recovery of the RRP after vesicle depletion by a high-frequency stimulus train (40 Hz for 2.5 s). Although there was a trend towards a slower EPSC recovery in synapses expressing DN- or KW-mutant Munc13-2, this effect was not statistically significant (Supplementary Fig. 8).

Synaptic but not non-synaptic Munc13 isoforms contain adjacent C_1- and C_2-domains similar to PKC, where they cooperate with each other[51]. At a synapse, phorbol esters increase the presynaptic vesicle release probability without changing the RRP size[47,52], at least in part by activating Munc13 (refs. 52 and 53). To test whether the Munc13 C_1- and C_2-domains also cooperate, we analyzed the effect of phorbol esters (1 μM PDBu applied for 1 min). We found that the relative potentiation by PDBu was significantly decreased in synapses expressing KW-mutant Munc13-2, whereas synapses expressing WT or DN-mutant Munc13-2 displayed similar degrees of potentiation (Figs. 6g). Plots of the relative potentiation of release by PDBu against the vesicular release probability for individual synapses revealed an inverse correlation (Fig 6h), indicating that the increased vesicular release probability caused by the KW-mutation occludes the PDBu potentiation.

DISCUSSION

Munc13's are essential components of the synaptic release machinery that prime synaptic vesicles for exocytosis, and regulate short-term plasticity of synaptic exocytosis[10,13,47,53,54], but their mechanisms of action remain unclear. Here, we show that the central C_2B-domain of Munc13's exhibits unusual Ca^{2+}- and PIP/PIP_2-dependent phospholipid binding properties. These properties structurally correlate with a unique accessory α-helix of the Munc13 C_2B-domain that is part of its Ca^{2+}-binding site. The unusual properties of the Munc13 C_2B-domain enable Munc13's to mediate Ca^{2+}-dependent augmentation of synaptic vesicle exocytosis during high-frequency trains of action potentials. As described below, we

believe that this augmentation is likely based on the Ca^{2+}-dependent binding of the Munc13 C_2B-domain to the plasma membrane, which in turn is enabled by increased synthesis of PIP and PIP_2 induced by accumulating Ca^{2+} during a high-frequency action potential train.

Properties of the Munc13 C_2B-domain

Structurally, the Munc13 C_2B-domain is composed of a standard C_2-domain β-sandwich in which aspartate residues in the `top' loops coordinate two Ca^{2+}-ions (Figs. 1 and 2). A distinctive feature of the Munc13 C_2B-domain is Ca^{2+}-binding loop 3, which includes an extended sequence that folds into an amphipathic α-helix (Fig. 2). Biochemically, the Munc13 C_2B-domain binds to phospholipids in a Ca^{2+}-dependent manner similar to other C_2-domains, but differs from other known C_2-domains, such as those from synaptotagmin, in that Ca^{2+}-dependent phospholipid binding requires relatively high concentrations of PIP or PIP_2 (Figs. 3 and 4). This unusual biochemical property is likely mediated, at least in part, by the unique α-helix formed by Ca^{2+}-binding loop 3, which contains a highly positively charged region that may act similarly to the PIP_2-dependent amphipathic α-helix observed in epsin[55].

Our data show that in addition to the amphipathic α-helix, the conserved, positively charged K630 residue in Ca^{2+}-binding loop 1 is a major determinant of the unusual phospholipid binding properties of the Munc13 C_2B-domain. In the Ca^{2+}-binding loops of synaptotagmin-1 C_2-domains, the residues analogous to K630 of Munc13 are hydrophobic (M173 and V304; Fig. 1a). During Ca^{2+}-dependent phospholipid binding of synaptotagmin-1 C_2-domains, M173 and V304 insert into the phospholipid bilayer, and contribute to the relatively non-specific but tight Ca^{2+}-dependent phospholipid-binding of these C_2-domains[38–41]. Moreover, exchanging M173 and V304 in the synaptotagmin-1 C_2-domains for tryptophan further enhances their Ca^{2+}-dependent phospholipid binding, indicating that tryptophan increases Ca^{2+}-dependent phospholipid binding mediated by hydrophobic residues[40,41,56]. These observations suggested to us that K630 in the Munc13 C_2B-domain may contribute to its unique specificity for high PIP/PIP_2-concentrations. To test this hypothesis, we substituted K630 of the Munc13 C_2B-domain for tryptophan, resulting in the KW-mutation. The KW-mutation rendered the Munc13 C_2B-domain responsive to PIP_2 at a concentration at which WT Munc13 is inert but synaptotagmin-1 is active, and thus confers synaptotagmin-like properties onto the Munc13 C_2B-domain (Fig. 4). As a result, the KW-mutation constitutes a gain-of-function mutation that enables Ca^{2+}-dependent binding of the Munc13 C_2B-domain to phospholipid membranes containing lower PIP/PIP_2-concentrations than the Munc13 C_2B-domain would normally bind to.

The C_2B-domain regulates synaptic plasticity

Strikingly, abolishing Ca^{2+}-binding to the Munc13-2 C_2B-domain with the DN-mutation did not alter vesicle exocytosis triggered by isolated action potentials (Fig. 5), but impaired facilitation of synaptic vesicle exocytosis induced by repeated action potentials (Fig. 6). Thus, the Munc13 C_2B-domain acts as a Ca^{2+}-regulator of short-term synaptic plasticity, consistent with the notion that synaptic facilitation during high-frequency stimulus trains is not passively caused by residual Ca^{2+}, but actively induced by Ca^{2+}-binding to the Munc13 C_2B-domain (and other Ca^{2+}-binding proteins). The KW-mutation, in contrast, increased the

amount of Ca^{2+}-triggered release during single and repeated action potentials (Figs. 5 and 6), without itself acting as a Ca^{2+}-sensor for release (Supplementary Fig. 7).

Viewed together, our data suggests that during isolated action potentials, the lower PIP/PIP_2-content at rest prevents Ca^{2+}-dependent binding of the WT Munc13 C_2B-domain to the membrane. During stimulus trains, a Ca^{2+}-dependent phosphatidylinositol kinase may increase the presynaptic PIP/PIP_2-content, allowing residual Ca^{2+} to activate Munc13 and thereby to boost release. Consistent with this hypothesis, Ca^{2+} stimulates PIP and PIP_2 synthesis in neuroendocrine cells[57], and depolarization of neurons activates presynaptic PIP kinase Iγ by dephosphorylation, thereby increasing the plasma membrane PIP/PIP_2-content[58–60]. Our hypothesis explains why the DN-mutation has no effect on Munc13 function during isolated action potentials, but interferes with Munc13 function during repeated action potentials. The hypothesis also accounts for the gain-of-function effect of the KW-mutation, since the PIP/PIP_2-content at rest is proposed to be too low to allow Ca^{2+}-activation of the WT Munc13 C_2B-domain, but may suffice for Ca^{2+}-activation of the KW-mutant C_2B-domain.

Mechanism of the Munc13 C_2B-domain action

In boosting release during a stimulus train, Ca^{2+}-binding to the Munc13 C_2B-domain likely increases vesicle priming by enhancing the priming function of Munc13. The KW-mutation may enable the Munc13 C_2B-domain to perform the same activity even at rest, possibly because the KW-mutant C_2B-domain binds to the plasma membrane even without the increase in PIP and PIP_2 concentrations that is thought to occur during repeated action potentials[57–60].

However, two of our findings with KW-mutant Munc13 appear to argue against the hypothesis that the Munc13 C_2B-domain boosts the priming function of Munc13:

1. the KW-mutation selectively increased the Ca^{2+}-sensitivity of release induced by isolated action potentials without increasing the size of the RRP (Fig. 5)
2. the KW-mutation did not significantly alter the rate by which evoked release recovered after depletion of the RRP, although there was a trend towards acceleration of priming (Supplementary Fig. 8)

Despite these findings, we believe that the priming hypothesis is correct for the following reasons: Priming likely involves a partial, if not complete assembly of SNARE-complexes between vesicles and the plasma membrane[61]. The number of assembled SNARE complexes per primed vesicle may determine (among others) the apparent Ca^{2+}-affinity of synaptic vesicle fusion[62]. Thus, Ca^{2+}-binding to the Munc13 C_2B-domain may increase the ability of Munc13 to catalyze SNARE-complex assembly of docked vesicles during priming, which would result in the appearance of an increased Ca^{2+}-sensitivity of release for the KW-mutation. This hypothesis is consistent with the fact that KW-mutant Munc13 does not act as a Ca^{2+}-sensor for exocytosis itself (Supplementary Fig. 7). Although plausible, the priming hypothesis cannot be tested directly until its underlying tenet – namely that Munc13 mediates vesicle priming by catalyzing SNARE-complex assembly – has been confirmed[63].

How does increased phospholipid binding induced by Ca^{2+}-binding to the Munc13 C_2B-domain potentiate Ca^{2+}-triggered release, be it via priming or otherwise? As a component of the biochemically insoluble active zone, Munc13 already is normally close to the plasma membrane. Thus, Ca^{2+}-dependent C_2B-domain binding to the plasma membrane would not re-localize Munc13, but rather pull on the adjacent plasma membrane and stretch it. Such an activity may, analogous to what has been proposed for the mechanism of action of synaptotagmin[64], promote exocytosis by decreasing the energy requirement for Ca^{2+}-triggered fusion-pore opening. DAG-binding to the C1-domain of Munc13 – which also induces Munc13 plasma membrane binding – may potentiate release by an analogous, but Ca^{2+}-independent mechanism. An alternative hypothesis is that the Munc13 C_1- and C_2B-domains are normally inhibitory, and that DAG- and Ca^{2+}-binding reverse this inhibition[54]. This second hypothesis would require that the C_1- and the C_2B-domain have additional unknown biochemical interactions beyond lipid binding which are altered by the various mutations, a possibility that remains to be explored.

Munc13 as a computational unit for synaptic transmission

The activity of synaptic Munc13 isoforms is regulated via three distinct, adjacent signaling motifs: the previously described calmodulin-binding sequence and C_1-domain[12,13], and the C_2B-domain we characterize here (Fig. 7). All three motifs are directly or indirectly activated by Ca^{2+}, and have profound roles in controlling neurotransmitter release during short-term plasticity, but differ from each other in their mechanisms of activation and action. The C_2B-domain is directly Ca^{2+}-activated by Ca^{2+}-influx during action potentials, but is presumably only stimulated after accumulating residual Ca^{2+} has induced the synthesis of PIP/PIP_2. In contrast, the calmodulin-binding sequence is indirectly activated by binding of accumulating residual Ca^{2+} to calmodulin, which likely acts on many synaptic targets simultaneously. The C_1-domain is activated indirectly via Ca^{2+}-dependent induction of phospholipase C. Thus, the Ca^{2+}-concentration dependence and time course of activation of the three regulatory motifs likely differ, leading to a common readout (synaptic potentiation) that results from the integration of multiple signals acting differentially on the three signaling motifs. Consistent with this model, the KW-mutation of Munc13 occludes the effect of phorbol esters on release triggered by isolated action potentials, whereas the DN-mutation (which has no effect on release triggered by isolated action potentials) has no effect on the phorbol ester potentiation under those conditions (Fig. 6). Moreover, at least mutations in the calmodulin-binding motif and the C_2B-domain act additively during short-term synaptic plasticity (Supplementary Fig. 9).

In summary, our data establish that the Munc13 C_2B-domain operates as a Ca^{2+}-regulator of short-term synaptic plasticity. Apart from the importance of the Munc13 C_2B-domain Ca^{2+}-binding properties for synaptic exocytosis, our results also suggest that this domain may act as a Ca^{2+}-regulator of exocytosis for non-synaptic Munc13 isoforms, which likely function in other forms of exocytosis (such as Munc13-4 in lymphocyte exocytosis[27]).

METHODS

Plasmids

Four different types of plasmids encoding rat Munc13-1 and 13-2 were used for this study: i. pGEX-KT derived plasmids for bacterial expression. ii. pFastBac™1 (Invitrogen life technologies) derived baculovirus expression plasmids into which we inserted the GST-coding region. The resulting plasmid was used for cloning pFastBac-GST-Munc13-1 C_2B (residues 675–820; numbering based on U24070); pFastBac-GST-Munc13-2 C_2B (residue 599–744; numbering based on AF159706); pFastBac-GST-Munc13-2 C_2B-DN (D629N and D635N); and pFastBac-GST-Munc13-2 C_2B-KW (K630W); iii. Semliki Forest Virus expression plasmids (pSFV ubMunc13-2 WT, pSFVubMunc13-2 C_2B-D629N,D635N, pSFVub Munc13-2K630W) for neuronal cultures. iv. Lentiviral expression plasmid pFUW-Munc13-2 K603W that encodes ubMunc13-2 with the KW mutation.

Production of recombinant proteins

1. Bacterial expression—GST fusion proteins were expressed at 25 °C in *E. coli* BL21, isolated by affinity chromatography on glutathione-Sepharose followed by on-resin cleavage with thrombin, and cleaved proteins were further purified by ion-exchange and gel-filtration chromatography on MonoS and S75 columns (Amersham). Uniform ^{15}N-labeling was achieved by growing the bacteria in $^{15}NH_4Cl$ as the sole nitrogen source.

2. Bacuolovirus expression—Munc13 C_2B-domain proteins were generated using Bac-to-Bac® Baculovirus Expression System (Invitrogen Life Technologies). Recombinant GST-Munc13 C_2B proteins were generated by infecting 400 ml of Sf9 cells (~2×10^6 cells/ml) in a 2 liter flask after inoculating 20 ml of baculovirus (~10^7 pfu/ml) for 3 days at 28 °C. Recombinant GST-fusion proteins were purified using glutathione-Sepharose™ 4B beads (Amersham Biosciences).

Antibodies were either described previously[2,3] or obtained from Synaptic Systems GmbH (Göttingen, Germany), except when stated otherwise. SDS-PAGE and immunoblotting were performed as described[3].

Fluorescence spectroscopy

Fluorescence spectra were recorded at 290 nm excitation in an LS55 luminescence spectrometer (PerkinElmer Life Sciences) with 0.3 μM purified Munc13 C_2B-domains in 0.5 ml of 20 mM HEPES-NaOH pH 7.2 and 0.1 M NaCl, with the indicated additions. All buffers were passed through the AG MP-50 resin (Bio-Rad) to eliminate contaminating Ca^{2+}.

NMR spectroscopy was carried out at 25 °C on Varian INOVA500 or INOVA600 spectrometers with samples containing ~120 μM Munc13-1 C_2B-domain (residues 675–820) in 20 mM MES-NaOH pH 6.2, 0.1 M NaCl, and 0.5 mM TCEP. Ca^{2+}-titrations were monitored by ^1H-^{15}N HSQC experiments as described[30]. All NMR data were processed with NMRPipe[65] and analyzed with NMRView[66].

X-ray crystallography

Purified Munc13-1 C_2B-domain (residues 675–820; in 20 mM MES-NaOH pH 6.2, 0.1 M NaCl and 0.5 mM TCEP) was concentrated to 20 mg/ml, and crystallized in 30% (w/v) PEG-MME 2000 and 0.1 M Bis-Tris-Propane pH 6.8 at 20 °C without Ca^{2+} or with 0.01–0.1 M $CaCl_2$ using the hanging-drop vapor-diffusion method. Ca^{2+}-free Munc13-1 C_2B-domain crystals appeared in two days, grew to a final size of 0.08 × 0.05 × 0.15 mm within a week, and were transferred into a solution of 35% (w/v) PEG-MME 2000, 0.1 M Bis-Tris-Propane pH 6.8 and 5% (v/v) glycerol, and flash-cooled in liquid propane. Ca^{2+}-bound Munc13-1 C_2B-domain crystals appeared within one week as needle-clusters and gradually transformed into a diamond-like shape over 3–4 weeks, with a final size of ~0.1 mm, after which they were transferred into a solution of 32% PEG-MME 2000, 0.1 M Bis-Tris-Propane pH 6.8, 0.1 M NaCl, 10% glycerol, 1 mM $CaCl_2$ and flash-cooled in liquid propane. Diffraction data were collected at the Structural Biology Center beamlines 19BM and 19ID of the Advanced Photon Source at 100K. The diffraction of these crystals was highly anisotropic, leading to a gradual decrease in the completeness at resolutions above 2.2 Å. Crystals of the Ca^{2+}-free Munc13-1 C_2B-domain diffracted to a d_{min} of ~1.89 Å (space group $C222_1$; unit cell parameters a = 43 Å, b = 101 Å, c = 68 Å; 1 molecule per asymmetric unit). Crystals of the Ca^{2+}-bound Munc13-1 C_2B-domain diffracted to a Bragg spacing (d_{min}) of ~1.37 Å (space group $P4_32_12$; unit cell parameters a = 57 Å, b = 57 Å, c = 90 Å, 1 molecule per asymmetric unit). Data were processed in the HKL2000 program suite[67]. The structure of the Ca^{2+}-free Munc13-1 C_2B-domain was determined via molecular replacement with the program AMoRe[68] using the synaptotagmin-1 C_2A-domain (PDB code 1rsy) as search model. The Ca^{2+}-bound Munc13-1 C_2B-domain structure was determined via molecular replacement with the program Phaser[69] using the final structure of Ca^{2+}-free Munc13-1 C_2B-domain as search model. Models were completed using the program Arp/Warp[70], followed by manual adjustments with the program O[71], and refinements with the program Refmac[72] of the CCP4 package[73], with a random subset of all data set aside for the calculation of free R factors. After complete refinement, solvent molecules were added where chemically reasonable. The final model for the Ca^{2+}-bound Munc13-1 C_2B-domain contains residues 673–675 and 687–819, two Ca^{2+}-ions, two Cl^--ions, one glycerol molecule, and 161 water molecules (final R = 17.0; R_{free} = 19.3; overall B-factor = 16.7). The final model for the Ca^{2+}-free Munc13-1 C_2B-domain contains residues 678–705, 708–763, 773–801 and 807–819, one molecule of Bis-Tris-Propane, 2 Cl^--ions, and 63 water molecules (final R = 21.7; R_{free} = = 28.2; overall B-factor = 41.0). For data collection and refinement statistics, see Table 1.

Phospholipid binding assays

1. Centrifugation assay—Phospholipids and cholesterol (obtained from Avanti) were dissolved in chloroform:methanol (1:1; cholesterol and PIPs) or chloroform (PS, PI, PC, and PE), mixed in a `synaptic' composition (41% PC, 32% PE, 12% PS, 5% PI, and 10% cholesterol with or without additional PIP and PIP_2; phospholipid composition approximates that of synaptic vesicles[13–15]), and dried under nitrogen. Lipids were resuspended by vortexing 175 mg lipid mixture for 20 min in 3.5 ml HEPES buffer (50 mM HEPES-NaOH pH 6.8, 0.1 M NaCl, and 4 mM EGTA) containing 0.5 M sucrose. Lipids were sonicated for

5 min in a bath sonicator (model G112SP1G; Laboratory Supply Co. Inc.), 14 ml HEPES buffer without sucrose were added, and liposomes were centrifuged at 100,000g for 30 min to separate heavy liposomes from free phospholipids. Liposomes were washed once, and repelleted (20,800g for 10 min). Binding assays were performed in 1 ml with 10 μg recombinant GST-fusion proteins (~0.125 μM) and 100 μg liposomes in HEPES buffer containing 2 mM $MgCl_2$ and various Ca^{2+}-concentrations that result in the indicated free [Ca^{2+}] as calculated with EqCal software (Biosoft, Ferguson, MI). Binding reactions were incubated 10 min at 30 °C with 800 rpm shaking, pelleted by centrifugation (20,800g for 10 min), and washed three times with 1 ml of the corresponding buffers. Final liposome pellets were dissolved in chloroform:methanol (1:2, v/v). Precipitated proteins were recovered by centrifugation (20,800g for 15 min), resuspended in 30 μl of 2× SDS sample buffer, and analyzed by SDS-PAGE and Coomassie Blue staining[2,16]. Bound proteins were quantified analysis of scanned Coomassie-stained gels with the Image Quant program (version 5.2, Molecular Dynamics).

2. FRET assays—were performed essentially as described[17] at room temperature in 0.5 ml of 20 ml HEPES-NaOH pH 7.2, 0.1 M NaCl, with 1 μM of Munc13-2 C_2B-domain protein and 30 μg/ml liposomes containing 41% PC, 22% PE, 10% dansyl-PE, 12% PS, 5% PI, 10% cholesterol, 0.5% PIP, and 0.1% PIP_2. Emission spectra (excitation: 282 nm) were first recorded without metal ions, then after addition of 2 mM $MgCl_2$, then after addition of 0.2 mM $CaCl_2$, and then after further addition of 1 mM EGTA.

GST pulldowns were performed as described[2]. One unstripped rat brain (~1.5 g/brain; Pel-Freez Biologicals, Rogers, Arkansas) was homogenized with a tissue homogenizer (Thomas Scientific, Philadelphia, Pennsylvania) in 30 ml HEPES buffer containing 1 mM DTT, 1 mM PMSF, 5 μg/ml leupeptin, and 2 μg/ml aprotinin. 1% Triton X-100 was added, proteins were extracted for 1 hr at 4 °C with rotation, insoluble proteins were removed by centrifugation (100,000g for 1 hr), and the supernatant was used for pulldowns using 30 μg GST-Munc13 C_2B-domain proteins attached to glutathione-Sepharose, and 0.5 ml rat brain lysate. Pulldown reactions (1 ml volume) in HEPES buffer containing 2 mM $MgCl_2$ and 0.5% Triton X-100 were incubated 1.5 hr at 4 °C with rotation, washed six times with corresponding buffer, and bound proteins were analyzed by SDS-PAGE and immunoblotting.

Electrophysiology

Microdot neuronal cultures were prepared and electrophopysiological analyses were performed at 22–25 °C as described[18–20,74]. Currents were recorded using an Axopatch 200B amplifier (Molecular Devices). Series resistance was within 10 MΩ and was electronically compensated at least 70%. Data were analyzed using AXOGRAPH software (version 4.9, Molcular Devices). For analyses of Syt-1 KO mice, primary cortical neurons from Syt-1 KO and littermate wild-type control mice were cultured in Modified Eagle Medium (MEM, Gibco) supplemented with B27 (Gibco), glucose, transferrin, fetal bovine serum, and Ara-C (Sigma)[74]. To monitor synaptic responses, whole-cell patch-clamp recordings were made with neurons at 14–16 days in vitro. Synaptic responses were triggered by a 1 ms current pulse (900 μA) through a local extracellular electrode (FHC,

Inc.), and recorded in whole-cell voltage-clamp mode using a Multiclamp 700B amplifier (Axon Instruments, Inc.)[74]. Data were analyzed using Clampfit 9.02 (Axon Instruments, Inc) or Igor 4.0 (Wavemetrics).

Statistical analyses were performed using paired Student's t-test or ANOVA.

Supplementary Material

Refer to Web version on PubMed Central for supplementary material.

ACKNOWLEDGEMENTS

We thank Ms. Izabela Kornblum, Ina Herfort, and Hui Deng for excellent technical support. This paper was supported by grants from the NIH (NS051262 to C.R.; NS40944 to J.R.) and the Deutsche Forschungsgemeinschat (to C.R.).

REFERENCES

1. Katz, B. The release of neuronal transmitter substances. Liverpool University Press; Liverpool, UK: 1969.
2. Abbott LF, Regehr WG. Synaptic computation. Nature. 2004; 431:796–803. [PubMed: 15483601]
3. Zucker RS, Regehr WG. Short-term synaptic plasticity. Annu. Rev. Physiol. 2002; 64:355–405. [PubMed: 11826273]
4. Mongillo G, Barak O, Tsodyks M. Synaptic theory of working memory. Science. 2008; 319:1543–1546. [PubMed: 18339943]
5. Brose N, Hofmann K, Hata Y, Südhof TC. Mammalian homologues of C. elegans unc-13 gene define novel family of C_2-domain proteins. J. Biol. Chem. 1995; 270:25273–25280. [PubMed: 7559667]
6. Wang Y, Okamoto M, Schmitz F, Hofman K, Südhof TC. RIM: A putative Rab3-effector in regulating synaptic vesicle fusion. Nature. 1997; 388:593–598. [PubMed: 9252191]
7. Betz A, et al. Functional interaction of the active zone proteins Munc13-1 and RIM1 in synaptic vesicle priming. Neuron. 2001; 30:183–96. [PubMed: 11343654]
8. Schoch S, et al. RIM1α forms a protein scaffold for regulating neurotransmitter release at the active zone. Nature. 2002; 415:321–326. [PubMed: 11797009]
9. Dulubova I, et al. A Munc13/RIM/Rab3 Tripartite Complex: From Priming to Plasticity? EMBO J. 2005; 24:2839–2850. [PubMed: 16052212]
10. Augustin I, et al. The cerebellum-specific Munc13 isoform Munc13-3 regulates cerebellar synaptic transmission and motor learning in mice. J. Neurosci. 2000; 21:10–17. [PubMed: 11150314]
11. Schlüter O, Schmitz F, Jahn R, Rosenmund C, Südhof TC. A complete genetic analysis of neuronal Rab3 function. J. Neurosci. 2004; 24:6629–6637. [PubMed: 15269275]
12. Rhee S-R, et al. Phorbol ester- and diacylglycerol-induced augmentation of neurotransmitter release from hippocampal neurons is mediated by Munc13s and not by PKCs. Cell. 2002; 108:121–133. [PubMed: 11792326]
13. Junge HJ, et al. Calmodulin and Munc13 form a Ca^{2+} sensor/effector complex that controls short-term synaptic plasticity. Cell. 2004; 118:389–401. [PubMed: 15294163]
14. Basu J, et al. A minimal domain responsible for Munc13 activity. Nat. Struct. Mol. Biol. 2005; 12:1017–1018. [PubMed: 16228007]
15. Xia Z, Storm DR. The role of calmodulin as a signal integrator for synaptic plasticity. Nat. Rev. Neurosci. 2005; 6:267–76. [PubMed: 15803158]
16. Zühlke RD, Pitt GS, Deisseroth K, Tsien RW, Reuter H. Calmodulin supports both inactivation and facilitation of L-type calcium channels. Nature. 1999; 399:159–162. [PubMed: 10335846]
17. Lee A, et al. Ca^{2+}/calmodulin binds to and modulates P/Q-type calcium channels. Nature. 1999; 99:155–159. [PubMed: 10335845]

18. DeMaria CD, Soong TW, Alseikhan BA, Alvania RS, Yue DT. Calmodulin bifurcates the local Ca^{2+} signal that modulates P/Q-type Ca^{2+} channels. Nature. 2001; 411:484–489. [PubMed: 11373682]
19. Wayman GA, Lee YS, Tokumitsu H, Silva A, Soderling TR. Calmodulin-kinases: modulators of neuronal development and plasticity. Neuron. 2008; 59:914–931. [PubMed: 18817731]
20. Sakaba T, Neher E. Calmodulin mediates rapid recruitment of fast-releasing synaptic vesicles at a calyx-type synapse. Neuron. 2001; 32:1119–1131. [PubMed: 11754842]
21. Huang YY, Li XC, Kandel ER. cAMP contributes to mossy fiber LTP by initiating both a covalently mediated early phase and macromolecular synthesis-dependent late phase. Cell. 1994; 79:69–79. [PubMed: 7923379]
22. Weisskopf MG, Castillo PE, Zalutsky RA, Nicoll RA. Mediation of hippocampal mossy fiber long-term potentiation by cyclic AMP. Science. 1994; 265:878–882.
23. Augustin I, Rosenmund C, Südhof TC, Brose N. Munc-13 is essential for fusion competence of glutamatergic synaptic vesicles. Nature. 1999; 400:457–461. [PubMed: 10440375]
24. Varoqueaux F, et al. Total arrest of spontaneous and evoked synaptic transmission but normal synaptogenesis in the absence of Munc13-mediated vesicle priming. Proc. Natl. Acad. Sci. USA. 2002; 99:9037–9042. [PubMed: 12070347]
25. Shiratsuchi T, et al. Cloning and characterization of BAP3 (BAI-associated protein 3), a C_2 domain-containing protein that interacts with BAI1. Biochem. Biophys. Res. Commun. 1998; 251:158–165. [PubMed: 9790924]
26. Koch H, Hofmann K, Brose N. Definition of Munc13-homology-domains and characterization of a novel ubiquitously expressed Munc13 isoform. Biochem. J. 2000; 349:247–253. [PubMed: 10861235]
27. Feldmann J, et al. Munc13-4 is essential for cytolytic granules fusion and is mutated in a form of familial hemophagocytic lymphohistiocytosis (FHL3). Cell. 2003; 115:461–473. [PubMed: 14622600]
28. Madison JM, Nurrish S, Kaplan JM. UNC-13 interaction with syntaxin is required for synaptic transmission. Curr. Biol. 2005; 15:2236–2242. [PubMed: 16271476]
29. Stevens DR, et al. Identification of the minimal protein domain required for priming activity of Munc13-1. Curr. Biol. 2005; 15:2243–2248. [PubMed: 16271475]
30. Ubach J, Zhang X, Shao X, Südhof TC, Rizo J. Ca^{2+} binding to synaptotagmin: how many Ca^{2+} ions bind to the tip of a C_2-domain? EMBO J. 1998; 17:3921–3930. [PubMed: 9670009]
31. Sutton RB, Davletov BA, Berghuis AM, Südhof TC, Sprang SR. Structure of the first C_2 domain of synaptotagmin I: a novel Ca^{2+}/phospholipid-binding fold. Cell. 1995; 80:929–938. [PubMed: 7697723]
32. Rizo J, Südhof TC. C_2-domains, structure and function of a universal Ca^{2+}-binding domain. J. Biol. Chem. 1998; 273:15879–15882. [PubMed: 9632630]
33. Shao X, Fernandez I, Südhof TC, Rizo J. Solution structures of the Ca^{2+}-free and Ca^{2+}-bound C_2A domain of synaptotagmin I: does Ca^{2+} induce a conformational change? Biochemistry. 1998; 37:16106–16115. [PubMed: 9819203]
34. Fernandez I, et al. Three-dimensional structure of the synaptotagmin 1 C_2B-domain. Synaptotagmin 1 as a phospholipid binding machine. Neuron. 2001; 32:1057–1069. [PubMed: 11754837]
35. Holm L, Sander C. Protein structure comparison by alignment of distance matrices. J. Mol. Biol. 1993; 233:123–138. [PubMed: 8377180]
36. Shao X, Davletov BA, Sutton RB, Südhof TC, Rizo J. Bipartite Ca^{2+}-binding motif in C_2 domains of synaptotagmin and protein kinase C. Science. 1996; 273:248–251. [PubMed: 8662510]
37. Benfenati F, Greengard P, Brunner J, Bahler M. Electrostatic and hydrophobic interactions of synapsin I and synapsin I fragments with phospholipid bilayer. J. Cell Biol. 1989; 108:1851–1862. [PubMed: 2497105]
38. Chapman ER, Davis AF. Direct interaction of a Ca^{2+} binding loop of synaptotagmin with lipid bilayers. J. Biol. Chem. 1998; 273:13995–14001. [PubMed: 9593749]
39. Zhang X, Rizo J, Südhof TC. Mechanism of phospholipid binding by the C_2A-domain of synaptotagmin I. Biochemistry. 1998; 37:12395–12403. [PubMed: 9730811]

40. Gerber SH, Rizo J, Südhof TC. Role of electrostatic and hydrophobic interactions in Ca^{2+}-dependent phospholipid binding by the C_2A-domain from synaptotagmin I. Diabetes. 2002; Suppl 1:2–8.
41. Shin OH, Rizo J, Südhof TC. Synaptotagmin function in dense core vesicle exocytosis studied in cracked PC12 cells. Nat. Neurosci. 2002; 5:649–656. [PubMed: 12055633]
42. Fernandez-Chacon R, et al. Synaptotagmin I functions as a calcium regulator of release probability. Nature. 2001; 410:41–49. [PubMed: 11242035]
43. Pang ZP, Shin OH, Meyer AC, Rosenmund C, Südhof TC. A gain-of-function mutation in synaptotagmin-1 reveals a critical role of Ca^{2+}-dependent soluble N-ethylmaleimide-sensitive factor attachment protein receptor complex binding in synaptic exocytosis. J. Neurosci. 2006; 26:12556–12565. [PubMed: 17135417]
44. Bennett MK, Calakos N, Scheller RH. Syntaxin: a synaptic protein implicated in docking of synaptic vesicles at presynaptic active zones. Science. 1992; 257:255–259. [PubMed: 1321498]
45. Li C, Ullrich B, Zhang ZZ, Anderson RGW, Brose N, Südhof TC. Ca^{2+}-dependent and Ca^{2+}-independent activities of neural and nonneural synaptotagmins. Nature. 1995; 375:594–599. [PubMed: 7791877]
46. Chapman ER, Hanson PI, An S, Jahn R. Ca^{2+} regulates the interaction between synaptotagmin and syntaxin 1. J Biol Chem. 1995; 270:23667–23671. [PubMed: 7559535]
47. Rosenmund C, et al. Differential control of vesicle priming and short-term plasticity by Munc13 Isoforms. Neuron. 2002; 33:411–425. [PubMed: 11832228]
48. Rosenmund C, Stevens CF. Definition of the readily releasable pool of vesicles at hippocampal synapses. Neuron. 1996; 16:1197–1207. [PubMed: 8663996]
49. Geppert M, et al. Synaptotagmin I: a major Ca^{2+} sensor for transmitter release at a central synapse. Cell. 1994; 79:717–727. [PubMed: 7954835]
50. Chapman PF, Frenguelli BG, Smith A, Chen CM, Silva AJ. The α-Ca^{2+}/calmodulin kinase II: a bidirectional modulator of presynaptic plasticity. Neuron. 1995; 14:591–597. [PubMed: 7695905]
51. Corbalan-Garcia S, Gomez-Fernandez JC. Protein kinase C regulatory domains: the art of decoding many different signals in membranes. Biochim. Biophys. Acta. 2006; 1761:633–654. [PubMed: 16809062]
52. Wierda KD, Toonen RF, de Wit H, Brussaard AB, Verhage M. Interdependence of PKC-dependent and PKC-independent pathways for presynaptic plasticity. Neuron. 2007; 54:275–290. [PubMed: 17442248]
53. Rhee SR, et al. Phorbol ester- and DAG-induced augmentation of neurotransmitter release from hippocampal neurons is mediated by Munc13s and not by PKCs. Cell. 2002; 108:121–133. [PubMed: 11792326]
54. Basu J, Betz A, Brose N, Rosenmund C. Munc13-1 C_1 domain activation lowers the energy barrier for synaptic vesicle fusion. J. Neurosci. 2007; 27:1200–1210. [PubMed: 17267576]
55. Ford MG, et al. Curvature of clathrin-coated pits driven by epsin. Nature. 2002; 419:361–366. [PubMed: 12353027]
56. Rhee J-S, et al. Augmenting neurotransmitter release by enhancing the apparent Ca^{2+}-affinity of synaptotagmin 1. Proc. Natl. Acad. Sci. U.S.A. 2005; 102:18664–18669. [PubMed: 16352718]
57. Eberhard DA, Holz RW. Calcium promotes the accumulation of polyphosphoinositides in intact and permeabilized bovine adrenal Chromaffin cells. Cell. Mol. Neurobiol. 1991; 11:357–370. [PubMed: 1651165]
58. Wenk MR, et al. PIP kinase Iγ is the major $PI(4,5)P_2$ synthesizing enzyme at the synapse. Neuron. 2001; 32:79–88. [PubMed: 11604140]
59. Itoh T, Ishihara H, Shibasaki Y, Oka Y, Takenawa. Autophosphorylation of type I phosphatidylinositol phosphate kinase regulates its lipid kinase activity. J. Biol. Chem. 2000; 275:19389–19394. [PubMed: 10777481]
60. Park SJ, Itoh T, Takenawa T. Phosphatidylinositol 4-phosphate 5-kinase type I is regulated through phosphorylation response by extracellular stimuli. J. Biol. Chem. 2001; 276:4781–4787. [PubMed: 11087761]
61. Südhof TC. The synaptic vesicle cycle: a cascade of protein-protein interactions. Nature. 1995; 375:645–653. [PubMed: 7791897]

62. Gerber SH, et al. Conformational switch of syntaxin-1 controls synaptic vesicle fusion. Science. 2008; 321:1507–1510. [PubMed: 18703708]
63. Rizo J, Rosenmund C. Synaptic vesicle fusion. Nat. Struct. Mol. Biol. 2008; 15:665–674. [PubMed: 18618940]
64. Martens S, Kozlov MM, McMahon HT. How synaptotagmin promotes membrane fusion. Science. 2007; 316:1205–1208. [PubMed: 17478680]
65. Delaglio F, et al. Nmrpipe - A Multidimensional Spectral Processing System Based on Unix Pipes. J. Biomol. NMR. 1995; 6:277–293. [PubMed: 8520220]
66. Johnson BA, Blevins RA. NMR View - A Computer-Program for the Visualization and Analysis of NMR Data. J. Biomol. NMR. 1994; 4:603–614. [PubMed: 22911360]
67. Otwinowski Z, Minor W. Processing of X-ray diffraction data collected in oscillation mode. Macromolecular Crystallography, Pt A. 1997; 276:307–326.
68. Navaza J. Amore - An Automated Package for Molecular Replacement. Acta Crystallographica Section A. 1994; 50:157–163.
69. McCoy AJ, Grosse-Kunstleve RW, Storoni LC, Read RJ. Likelihood-enhanced fast translation functions. Acta Crystallogr. D. Biol. Crystallogr. 2005; 61:458–464. [PubMed: 15805601]
70. Perrakis A, Harkiolaki M, Wilson KS, Lamzin VS. ARP/wARP and molecular replacement. Acta Crystallogr. D. Biol. Crystallogr. 2001; 57:1445–1450. [PubMed: 11567158]
71. Jones TA, Zou JY, Cowan SW, Kjeldgaard M. Improved Methods for Building Protein Models in Electron-Density Maps and the Location of Errors in These Models. Acta Crystallographica Section A. 1991; 47:110–119.
72. Murshudov GN, Vagin AA, Dodson EJ. Refinement of macromolecular structures by the maximum-likelihood method. Acta Crystallographica Section D-Biological Crystallography. 1997; 53:240–255.
73. Collaborative Computational Project No. 4. The CCP4 suite: programs for protein crystallography. Acta Crystallogr. D Biol. Crystallogr. 1994; 50:760–763. [PubMed: 15299374]
74. Pyott SJ, Rosenmund C. The effects of temperature on vesicular supply and release in autaptic cultures of rat and mouse hippocampal neurons. J. Physiol. 2002; 539:523–535. [PubMed: 11882684]
75. Maximov A, Pang Z, Tervo DGR, Südhof TC. Monitoring Synaptic Transmission in Primary Neuronal Cultures Using Local Extracellular Stimulation. J. Neurosci. Methods. 2007; 161:75–87. [PubMed: 17118459]

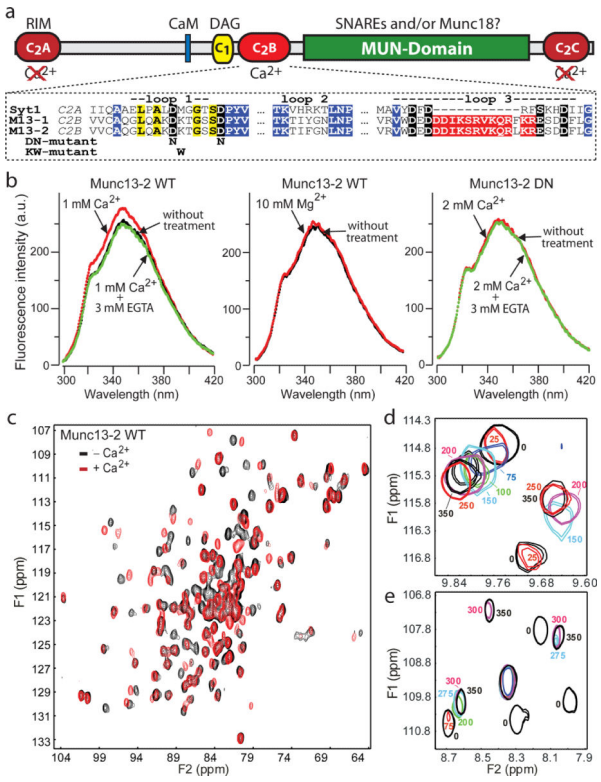

Figure 1. The Munc13-1 C_2B-domain is a Ca^{2+}-binding module

a. Domain organization of Munc13-1 and bMunc13-2. The binding activities of various domains are indicated above (CaM = calmodulin; DAG = diacylglycerol), and their presumed Ca^{2+}-binding ability below the domains. An alignment of the Ca^{2+}-binding loops from the synaptotagmin-1 C_2A-domain, the Munc13-1 C2B-domain, and the Munc13-2 C_2B-domain is shown below the domain organization (residues 162–241 from rat synaptotagmin-1 [acc. # X52772]; 695–779 from rat Munc13-1 [acc. # U24070]; and 619–703 from rat bMunc13-2 [acc. # AF159706]). In the alignment, conserved sequences are highlighted (black = Ca^{2+}-binding residues; yellow = top loop; blue = β-strands; red = conserved charged sequence in loop 3 specific for the Munc13 C_2B-domains). The two C_2B-domain mutations analyzed ("DN" and "KW") are described at the bottom.

b. Fluorescent emission spectra of WT and DN-mutant Munc13-2 C_2B-domains without and with 1 mM Ca^{2+} plus/minus EGTA, or with 10 mM Mg^{2+} (for data on Munc13-1 and for individual spectra, see Supplementary Fig. 1).

c. ^1H-^{15}N HSQC spectra of the Munc13-1 C_2B-domain in the absence (black contours) and presence (red contours) of 0.5 mM Ca^{2+}.

d, ***e***. Ca^{2+}-binding to the Munc13-1 C_2B-domain monitored with ^1H-^{15}N HSQC spectra. The diagrams show expansions of superpositions of selected ^1H-^{15}N HSQC spectra acquired during a titration of Ca^{2+} from 0 to 0.7 mM. The contours are color coded according to the Ca^{2+}-concentration (indicated in μM next to the contours).

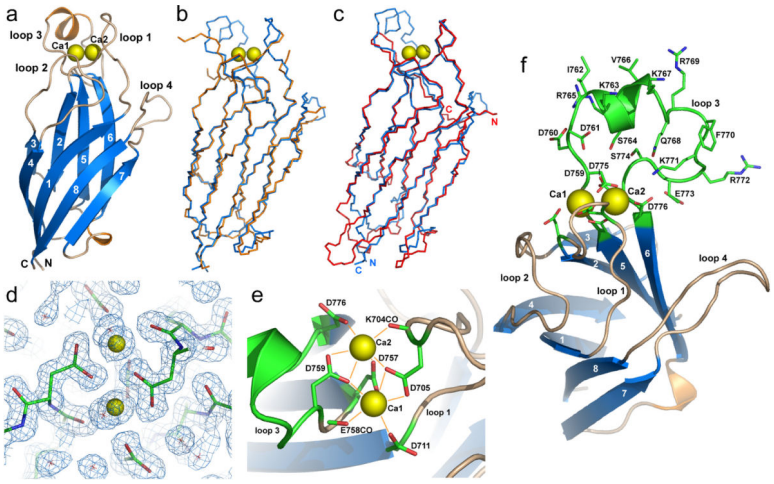

Figure 2. Three-dimensional structures of the Ca^{2+}-free and Ca^{2+}-bound Munc13-1 C_2B-domain

a. Ribbon diagram of the crystal structure of the Ca^{2+}-bound Munc13-1 C_2B-domain (blue = β-strands; orange = α-helices). Bound Ca^{2+}-ions are shown as yellow spheres; β-strands are numbered from 1 to 8. The top loops are labeled loop 1 – loop 4; N and C indicate N- and C-termini, respectively. See Supplementary Fig. 2 for analysis of crystal contacts.

b. Backbone superposition of the Ca^{2+}-free (orange) and Ca^{2+}-bound (blue) Munc13-1 C_2B-domains.

c. Backbone superposition of the crystal structures of the Ca^{2+}-bound Munc13-1 C_2B-domain (blue) and the Ca^{2+}-free synaptotagmin-1 C_2A-domain (red; PDB accession code 1rsy). N- and C-termini of both domains are indicated with letters of the corresponding color.

d. 2Fo−Fc electron density map contoured at 1σ of the Ca^{2+}-binding region of the Munc13-1 C_2B-domain superimposed with a stick model of the protein. Ca^{2+}-ions and water molecules are represented by yellow spheres and red stars, respectively. In this and the following panels, protein atoms are color coded: green, carbon; blue, nitrogen; red, oxygen.

e. Ribbon-and-stick diagram summarizing the Ca^{2+}-binding mode of the Munc13-1 C_2B-domain. The water molecules are not shown for simplicity. All other Ca^{2+}-ligands are shown as stick models and labeled; K704CO and E758CO denote the backbone carbonyl group of the corresponding residues. Ca^{2+}-ions are labeled Ca1 and Ca2.

f. Ribbon-and-stick diagram of the Munc13-1 C_2B-domain illustrating the amphipathic character of the α-helix of loop 3. The side chains of the Ca^{2+} ligands and of all residues in loop 3 are shown as stick models.

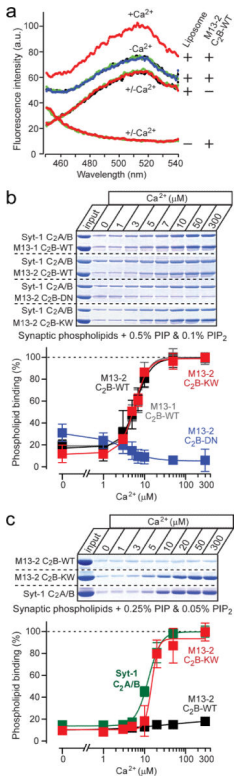

Figure 3. Ca^{2+}-dependent binding of the Munc13 C_2B-domain to PIP/PIP_2-containing liposomes

a. FRET assays of Ca^{2+}-dependent binding of the Munc13 C_2B-domain to dansyl-labeled `synaptic' liposomes containing 0.5% PIP and 0.1% PIP_2 (0.03 mg/ml; total volume = 0.6 ml). Fluorescence spectra (excitation = 282 nm) were monitored in solutions containing either only the C_2B-domain, liposomes, or both as indicated on the right[34]. Spectra were first recorded in Ca^{2+}-free buffer (black traces, covered by overlying green, red, or blue traces), then after addition of 2 mM Mg^{2+} (blue traces, under the overlying green or red traces), then after addition of 0.2 mM Ca^{2+} (red traces), then again after further addition of 1 mM EGTA (green trace, done only for the samples containing both liposomes and C_2B-domain protein). Data show a representative experiment repeated multiple times; see Supplementary Fig. 3 for individual spectra.

b, c. Centrifugation assays of Ca^{2+}-dependent Munc13 C_2B-domain binding to `synaptic' liposomes containing 0.5% PIP and 0.1% PIP_2 (b), or 0.25% PIP and 0.05% PIP_2 (c). GST-fused Munc13 C_2B-domains and the synaptotagmin-1 C_2A/B-domain fragment (used as an internal control) were bound to liposomes at the indicated free Ca^{2+}-concentrations clamped with Ca^{2+}/EGTA buffer containing 2 mM Mg^2. Co-pelleted Munc13 and synaptotagmin-1 C_2-domains were analyzed by SDS-PAGE and Coomassie Blue staining, and quantified by scanning (top panels = representative experiments; bottom panels = summary graphs (means ± SEMs [n=3]); data were normalized to binding at the highest Ca^{2+}-concentration; quantitations for synaptotagmin-1 for panel b are shown in Supplementary Fig. 4).

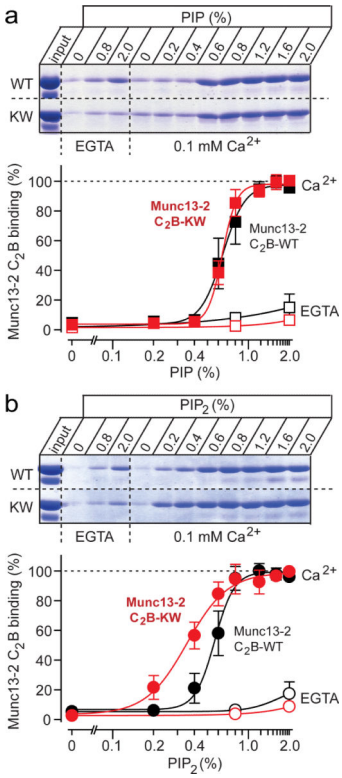

Figure 4. PIP- and PIP_2-dependence of Ca^{2+}-induced liposome binding to Munc13 C_2B-domains

a, b Quantitation of Ca^{2+}-dependent Munc13 C_2B-domain binding to `synaptic' liposomes as a function of the PIP- (a) or PIP_2-concentration (b). Binding assays were carried out using the centrifugation assay (Figs. 3b and 3c) in the absence (open symbols) or presence of 0.1 mM Ca^{2+} (filled symbols) as a function of the concentration of PIP (a) or PIP_2 (b) in the liposomes. The top panels display representative experiments, and the bottom panels summary graphs (means ± SEMs [n=3]; data were normalized to binding at the highest free Ca^{2+} concentration). Wild-type and KW-mutant C_2B-domains are not significantly different for the PIP titration (a), but are significantly different for the PIP_2 titration (b; p=0.0016 using a 2-way ANOVA test; see Supplementary Fig. 5 for direct comparison of the binding of the WT C_2B-domain to PIP- or PIP_2-containing liposomes).

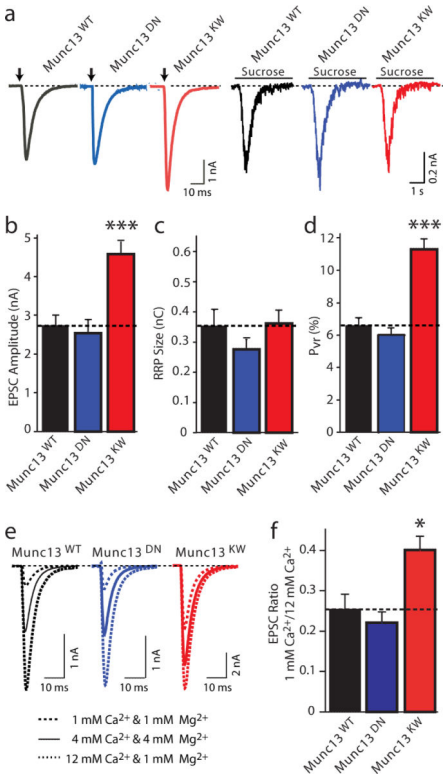

Figure 5. Effect of Munc13-2 C_2B-domain mutations on release induced by isolated action potentials

All experiments in this figure and Fig. 6 were performed in hippocampal autaptic neurons cultured from Munc13-1/-2 double KO mice. Neurons were infected with recombinant Semliki Forest Virus expressing WT, DN-mutant, or KW-mutant Munc13-2, and excitatory postsynaptic currents (EPSCs) were recorded in whole-cell mode.

a, Representative EPSCs evoked by isolated action potentials (left) or 0.5 M sucrose (right) in neurons expressing WT (black), DN-mutant (blue), or KW-mutant Munc13-2 (red).

b–d, Mean EPSC amplitudes (b), RRP size (c, measured as the response to 0.5 M sucrose, integrating the transient current component for 4 s); and vesicular release probability (d, calculated as the ratio of the charge of evoked responses to that of the RRP). Data shown are means ± SEMs (n= (WT: n=58; DN: n=57; KW: n=79; ***, $p<0.001$ by paired t-test).

e, Representative EPSCs evoked by isolated action potentials in neurons expressing WT (black), DN-mutant (blue), or KW-mutant Munc13-2 (red) at three different Ca^{2+}-concentrations as indicated.

f, Mean ratio of the EPSC amplitudes monitored at low vs. high Ca^{2+} in neurons expressing WT (black), DN-mutant (blue), or KW-mutant Munc13-2 (red; WT, n=16; DN, n=14; KW, n=16; *, $p<0.05$; see Supplementary Table 2 for a numerical listing of all electrophysiologically results.

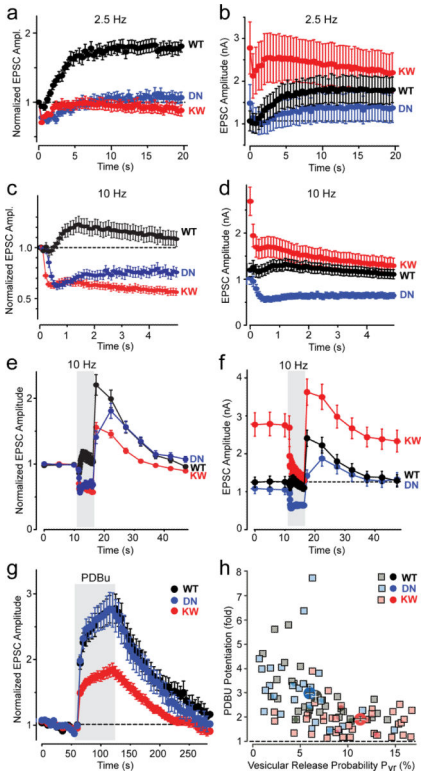

Figure 6. Ca^{2+}-binding to the Munc13 C_2B-domain regulates release during high-frequency action potential trains

a, b. Mean normalized (left panels) and absolute (right panels) EPSC amplitudes in response to a 2.5 Hz (a) or 10 Hz (b) action potential train in Munc13-deficient neurons expressing WT (black), DN-mutant (blue), or KW-mutant Munc13-2 (red; means ± SEMs). In the normalized plots (left panels), $p<0.001$ for WT compared to DN- and KW-mutant Munc13-2; in the absolute responses (right panels), the initial responses are significantly larger ($p<0.01$) for the KW-mutant Munc13-2 compared to the WT or DN-mutant protein, whereas the final responses are significantly smaller ($p<0.001$) for the DN-mutant compared to the WT and KW-mutant Munc13-2 (2.5 Hz, WT n=18; KW n=21; DN; n=16; 10 Hz, WT n=50; DN n=41; KW n=64).

c., d. Normalized (c) and absolute EPSC amplitudes (d) in response to a low-frequency stimulus train (0.2 Hz) that is interrupted by a 5 sec 10 Hz stimulus train to induce augmentation (gray area)[47]. Munc13-deficient neurons expressing WT (black), DN-mutant (blue), or KW-mutant Munc13-2 (red) were analyzed (for normalized responses, degree of augmentation is significantly higher ($p<0.001$) for WT compared to DN- and KW-mutant Munc13-2; for absolute responses, all three Munc13 forms differ significantly from each other at the $p<0.001$ level (WT n=50; DN n=41; KW n=64)).

e. Relative potentiation by PDBu (1 μM) of EPSC amplitudes evoked at 0.2 Hz in Munc13-deficient neurons expressing WT (black), DN-mutant (blue), or KW-mutant Munc13-2 (red). The relative PDBu potentiation was significantly lower ($p<0.001$) in synapses expressing KW-mutant Munc13-2 than in synapses expressing WT or DN-mutant Munc13-2 (WT, n=30; DN, n=31; KW, n=43).

f. Plot of the degree of PDBu potentiation as a function of the initial vesicular release probability (P_{vr}) in individual neurons. Each individual data point represents a Munc13-deficient neuron expressing WT (black), DN-mutant (blue), or KW-mutant Munc13-2 (red). The solid symbols represent the mean values for each group.

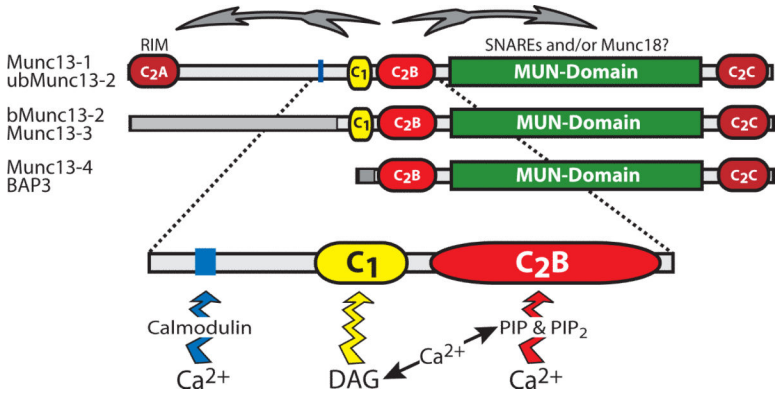

Figure 7. Model for the Ca^{2+}-regulation of short-term plasticity by Munc13

The top diagrams depict the domain structures of the three sub-families of Munc13 proteins, the two classes of long Munc13s expressed primarily in brain, and the class of short Munc13s expressed primarily in peripheral organs. Top arrows illustrate a possible regulation of the N-terminal RIM-binding sequences and the C-terminal MUN-domain of Munc13s by ligand-binding to the central C_1- and C_2-domains. The central regulatory domains of Munc13's are illustrated below the domain diagrams: the calmodulin-binding sequence found in Munc13-1 and bMunc13-2, the DAG-binding C_1-domain found in all variants of Munc13-1, -2, and -3 but not the ubiquitous Munc13 isoforms, and the Ca^{2+}-binding C_2B-domain that is universally present in all neuronal and ubiquitous Munc13 isoforms. Note that in addition to binding to the C_2B-domain, Ca^{2+} also serves to stimulate the production of DAG from PIP_2 on the one hand, and the synthesis of DAG on the other hand.

Table 1

Data collection and refinement statistics for the Munc13-1 C_2B domain

	Munc13-1 C_2B-domain Ca^{2+}-free	Munc13-1 C_2B-domain Ca^{2+}-bound
Data collection		
Space group	$C222_1$	$P4_32_12$
Cell dimensions		
a, *b*, *c* (Å)	42.57, 101.14, 68.04	55.94, 55.94, 89.98
α, β, γ (°)	90.0, 90.0, 90.0	90.0, 90.0, 90.0
Resolution (Å)*	26.43-1.90 (1.93-1.90)	30.00-1.37 (1.39-1.37)
R_{merge} (%)	5.0 (37.9)	5.5 (46.4)
$I/\sigma I$	33.1 (2.4)	40.8 (3.1)
Completeness (%)	86.5 (47.5)	99.8 (96.4)
Redundancy	7.5 (3.3)	12.6 (6.1)
Refinement		
Resolution (Å)	26.00 – 1.90 (1.94-1.90)	30.00 – 1.37 (1.40-1.37)
No. reflections (unique/R_{free})	9,905/501	30,262/1,546
R_{work} / R_{free}	0.217 (0.263) / 0.282 (0.318)	0.170 (0.208) / 0.193 (0.231)
No. atoms	1,019	1,352
Protein	935	1,175
Ligand/ion	19/2	12/4
Water	63	161
B-factors		
Protein	43.9	17.3
Ligand/ion	45.7/49.0	14.7/15.5
Water	45.9	18.4
R.m.s. deviations		
Bond lengths (Å)	0.017	0.018
Bond angles (°)	1.579	1.813

For each structure, data was collected from one crystal.

*Values in parentheses are for highest-resolution shell.